frontiers | Frontiers in Energy Research

TYPE Original Research
PUBLISHED 18 January 2024
DOI 10.3389/fenrg.2024.1327955

OPEN ACCESS

EDITED BY
Xu Liu,
Helmholtz-Institut Ulm (HIU), Germany

REVIEWED BY
Yuxiao Lin,
Jiangsu Normal University, China
Xu Dong,
Karlsruhe Institute of Technology (KIT), Germany

*CORRESPONDENCE
Corey T. Love,
corey.love@nrl.navy.mil

†These authors have contributed equally to this work

RECEIVED 25 October 2023
ACCEPTED 08 January 2024
PUBLISHED 18 January 2024

CITATION
Raj A, Atkinson RW III, Kingston TA, Carter R and Love CT (2024), Thermal gradient strategy to improve seeding for high rate zero excess lithium metal batteries.
Front. Energy Res. 12:1327955.
doi: 10.3389/fenrg.2024.1327955

Thermal gradient strategy to improve seeding for high rate zero excess lithium metal batteries

Abhi Raj[1,2†], Robert W. Atkinson III[3†], Todd A. Kingston[4], Rachel Carter[1] and Corey T. Love[1*]

[1]Chemistry Division, U.S. Naval Research Laboratory, Washington, DC, United States, [2]ASEE/NRL Postdoctoral Fellow, U.S. Naval Research Laboratory, Washington, DC, United States, [3]Excet, Inc., Springfield, VA, United States, [4]Department of Mechanical Engineering, Iowa State University, Ames, IA, United States

Zero excess lithium metal batteries (LMBs) have traditionally suffered from short cycle life due to nonuniform processes that result in parasitic side reactions and a subsequent loss of lithium inventory and electrolyte. The experiments herein demonstrate that zero excess LMB cells cycled with a low thermal average and thermal gradient outperform cells cycled under isothermal conditions during early cycles. Specifically, a low thermal average of ~6.4°C and thermal gradient of <1°C across the cell is shown to increase the overpotential for lithium deposition at the anode current collector, likely resulting in smaller and higher density nucleates, providing film like morphologies observed with microscopy. Improved performance from this approach is demonstrated at high cycling rates (>4C) and mismatched charge/discharge rates. Optimal cycling behavior was observed with 2C charging (30 min) and 3C discharging (20 min). These advantages were translated to the system relevant form factor-pouch cell (20X capacity). Based on the performance enhancement observed with extended application of a thermal gradient, we demonstrate the use of the environment as a formation strategy, to perpetuate improved plating in stripping over the cycle life of zero excess LMBs operating in ambient conditions.

KEYWORDS

zero excess lithium, lithium metal, battery, safety, thermal gradient, cycle life, impedance spectroscopy, concentrated electrolyte

1 Introduction

Lithium-ion batteries are the workhorse energy storage technology for a range of applications, spanning from transportation to consumer electronics. As such applications increase in their energy demands, researchers have sought to move beyond the intercalation structures such as graphite, which are required to host lithium ions. Through direct electroplating and stripping at the anode, metallic lithium offers a high specific capacity (3860 mA h g^{-1}) and a reduction potential of −3.05 V *versus* a standard hydrogen electrode, thereby resulting in the ideal high capacity anode for high-energy-density batteries. To leverage that energy density as well as overcome the manufacturing issues associated with fabricating and handling thin lithium foils, zero excess lithium cell configurations utilize lithium provided by the cathode as the sole source of lithium inventory in the cell (Qian et al., 2016; Nanda et al., 2020; Hatzell, 2023; Lohrberg et al., 2023). Traditionally, these

systems have suffered from short cycle life due to parasitic side reactions that lead to consumption of lithium ion inventory and electrolyte depletion (Liao et al., 2005; Nanda et al., 2020; Zhao et al., 2023). These side reactions are exacerbated by nonuniform lithium deposition at the anode which can also result in safety concerns as volume changes associated with plating and stripping may lead to isolated metallic lithium that contributes to an increased severity of thermal runaway processes.

In their review of the field, Nanda et al. broadly classifies strategies to improve the cycle life of ZELMBs in three categories: (i) electrolyte optimization, (ii) current collector modification, and (iii) formation/cycling parameters (Nanda et al., 2020). In each of these cases, the underlying motivation is to promote uniform deposition and stripping of metallic lithium at the anode surface in order to mitigate lithium inventory loss. Broadly, efforts in electrolyte design and current collector modification have aimed to improve deposition morphology and consequentially, facilitate higher plating efficiencies (Nilsson et al., 2019; Nanda et al., 2020). Electrolyte design also facilitates the decomposition of electrolyte into a favorable solid electrolyte interface (SEI) (Zhang et al., 2022; Park et al., 2023). Specifically, highly concentrated electrolytes have been used to form SEIs that result in improved interactions with the lithium (Li) anode through their intrinsic properties of increased Li^+ diffusivity, concentration, and transference number (Nilsson et al., 2019). In other cases, electrolytes have been developed and additives introduced to promote cell operation in a range of temperatures (Zhang et al., 2023). This type of research is vital towards not only ensuring operation under real world conditions, but also in enabling temperature control as an operational strategy to improve cell performance. The experiments in this study rely on such an electrolyte designed to enable low temperature operation designed by Thenuwara et al. (2020).

This work also builds on a growing literature focused on optimizing current collectors in order to promote better seeding and nucleation of lithium (Yan et al., 2016; Pei et al., 2017). In the study by Yan et al. (2016), metals exhibiting solubility in lithium (e.g., Au) are shown to present no nucleation barriers to lithium growth; for copper (Cu), the mismatch in crystal structure between Li and Cu results in a ~40 mV overpotential in order to overcome a nucleation barrier. In the work by Pei et al. (2017), increasing current rates are shown to result in increased overpotentials and accordingly, densely distributed Li nuclei. This principle of using increased overpotentials for modulating the plating morphology is corroborated in this work not only through variations in current density, but also through temperature control, i.e., a thermal gradient condition at a low thermal average, during formation and/or cycling.

Formation and cycling parameters ranging from electrochemical protocols to temperature and pressure have long been shown as ways to benefit cell lifetime (Qian et al., 2016). More recently, Louli et al. (2021) demonstrated that an asymmetry in charge and discharge rates proves to be more important than the absolute current densities Specifically, discharging at faster rates generates a concentration gradient at the lithium surface which thereby results in preferential stripping of lithium protrusions at the anode, leaving behind a uniform surface at the end of discharge. This strategy is employed throughout the experiments in this work such that the discharge rate ranges from 1 to 2× the charge rate.

Beyond electrochemical protocols, temperature is an effective lever in modulating performance in Li-ion cells; in some cases it is used to improve cycle life and in others, accelerate degradation. By cycling Li-ion cells at elevated temperatures, many studies have sought to balance the tradeoff between improved diffusion and increased rates of parasitic reactions (Chang et al., 2021). Indeed, previous efforts in our group revealed that isothermal cycling at warm or cold temperatures has a direct impact on lithium diffusion and the ability to form a stable SEI (Carter and Love, 2018; Atkinson et al., 2019; Mistry et al., 2019; Atkinson et al., 2020). Temperature effects on cycling lithium metal coin cells have also demonstrated improved electroplating reversibility at higher temperatures due to improved lithium diffusion and a more favorable SEI formation (Wang et al., 2019; Yan et al., 2019). Previous efforts in our group demonstrated that an interelectrode thermal gradient, defined as a temperature difference between a cathode and anode, accelerated degradation by inducing early lithium plating on graphite anodes in conventional Li-ion cells (Carter and Love, 2018). When considering symmetric lithium metal cells, our group has found that a positive thermal gradient in the first half-cycle (warmer electroplating electrode and colder stripping electrode) induced preferential deposition of lithium during early cycling and resulted in longer cycle life as compared to cells in which a negative thermal gradient was applied, or even those cycled isothermally at 20 or 0°C (Atkinson et al., 2019; Atkinson et al., 2020). In the latter study, operando optical microscopy revealed that the isothermal 20 C condition results in larger lithium features and dendritic growth while the positive thermal gradient at a low thermal average results in smaller, rounded, and more homogeneous deposits. It was also shown that a positive thermal gradient centered at 21°C outperformed the isothermal 20°C condition, confirming the benefit of the thermal gradient for cells with equivalent thermal averages. These results have motivated a recent study demonstrating the importance of homogeneous distribution of heat to prevent the nucleation and growth of lithium dendrites (Atkinson et al., 2020). This work focuses on the positive thermal gradient at a low thermal average, with an isothermal warm condition selected as a control as this condition is the standard in literature for cycle life testing (room temperature with no active thermal control). While Li-metal literature generally favors cycling at elevated temperatures, operation at a lower temperature results in formation of a thinner, less resistive SEI wherein the SEI composition and structure are also more favorable; such a compact and inorganic-rich SEI has been shown to improve Li-ion transport and electrode stability (Thenuwara et al., 2019; Thenuwara et al., 2020; Yang et al., 2019). More broadly, previous investigations on temperature effects on LMB performance have found that prolonged cycling at elevated temperatures likely leads to considerable gas formation and that temperature modulation is most effective as a formation strategy; in one such study, two formation cycles at 40 C were shown to result in dense, columnar growth of lithium at the anode as compared to cells cycled at 20°C (Genovese et al., 2019). In a similar vein, the aforementioned interelectrode thermal gradient strategy presents an opportunity to build on prior literature that uses temperature as a way to improve performance through the modulation of lithium plating and morphology.

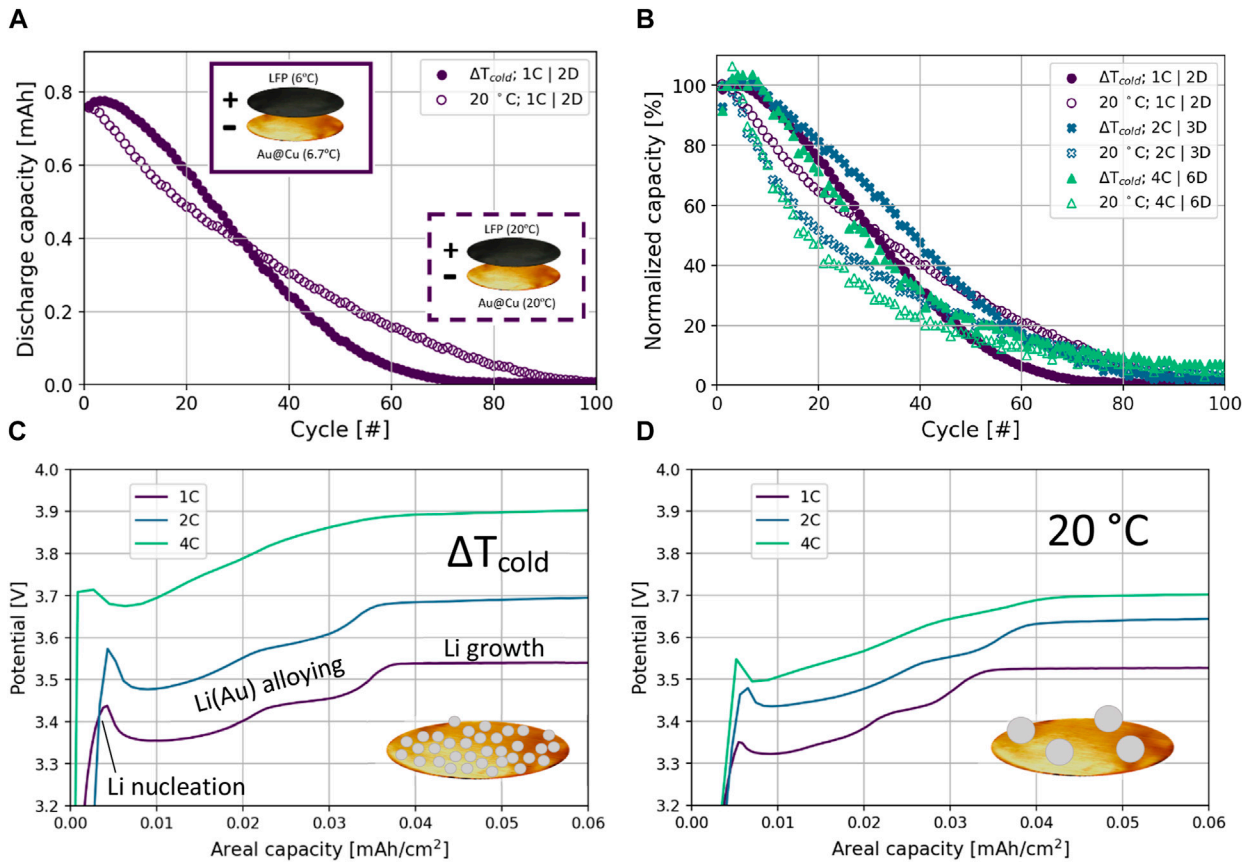

FIGURE 1
(A) Comparison of discharge capacity during 1C|2D cycling using the thermal gradient strategy (ΔT_{cold}) and cycling at 20°C; schematic of ΔT_{cold} inset (solid line) and 20°C isothermal (dashed line); the height of the y-axis corresponds to 0.909 mA h, the theoretical capacity of the cathode. **(B)** Comparison of normalized capacity for ΔT_{cold} and 20°C cells. **(C,D)** are voltage profiles during the initial portion of the first charge for ΔT_{cold} and 20 C conditions, respectively. As shown in the inset of **(C)**, the higher overpotential for Li nucleation for the ΔT_{cold} cells likely results in a higher density of smaller nucleates on the anodic current collector which promotes a dense layer for continued plating and stripping, as compared to the large and sparse nucleates depicted in the inset of **(D)**.

To that point, this work will present the use of thermal gradients as a strategy to improve early cycling performance of zero excess lithium metal cells. With the hypothesis that these enhancements are related to seeding morphology, we examine the use of applying a thermal gradient during only the formation cycles to provide (i.e., seed) more suitable plating behaviors perpetuated in subsequent cycles. We also explore the combination of the thermal gradient strategy with other factors, such as increased electrolyte concentration or current collector modification. Moreover, by demonstrating that even minor internal thermal gradients have a major impact on cell performance, either for better or worse, this work motivates careful consideration of thermal regulation in future cell or pack designs that incorporate Li metal cells.

2 Results and discussion

2.1 Thermal gradient impacts on anode-free cycle life

A direct comparison between ZELMBs, featuring $LiFePO_4$ (LFP) cathode (1C = 0.909 mA h) and 25 nm gold (Au) coating on a Cu foil anode, using the thermal gradient strategy (ΔT_{cold}) and those cycled isothermally at 20 C is displayed in Figure 1A. In the ΔT_{cold} condition, the current collector of the positive electrode, LFP cathode, is maintained at 6°C and the current collector of the negative electrode, Au@Cu, at 6.7°C. An inset illustrating these thermal conditions is provided in Figure 1A and a schematic of the experimental setup in Supplementary Figures S1A. Through the first 30 cycles, ΔT_{cold} cells outperform cells cycled at 20 C as the former exhibits slower initial capacity fade. This behavior is consistent at increased cycling rates, illustrated in Figure 1B, which displays normalized capacity based on the cycle 1 discharge in order to directly compare rate-dependent capacities. In this figure, it is helpful to note that charge and discharge C-rates are noted as C/x and D/x, respectively, where x is the number of hours to complete a full charge or discharge. Corresponding discharge capacity curves for these cycling conditions are provided in Supplementary Figures S2A. From these initial capacity curves as well as analysis of coulombic efficiency as provided in Supplementary Figures S2B, it is expected that the stripping efficiency of the plated Li was enhanced for the cells subjected to the thermal gradient cells during initial cycling, but this benefit diminished as cycling continued. After ~60 cycles, the capacity delivered by any cell is

so small, making the coulombic efficiency measurement meaningless.

The combination of both a low thermal average and thermal gradient in the ΔT_{cold} condition outperforms the isothermal 20°C cell during early cycling. It is generally accepted that cold, isothermal conditions favor dendritic growth, early shorting, and poor performance (Love et al., 2014). From this, we suggest that the stable cycling demonstrated is not a result of the low thermal average alone. In previous efforts, our research group has shown that a thermal gradient at a ~21°C thermal average was more stable than isothermal 20 C in symmetric Li-metal cells (Atkinson et al., 2019). This effort also demonstrates that a cold thermal gradient leads to better stability than the warmer thermal gradient centered near 21 °C. Modeling efforts focused on understanding the relationship between applied thermal gradients and electroplating have also shown that surface Li diffusion is enhanced to form uniform electrodeposits when the electroplating electrode is warmer than the stripping electrode (Mistry et al., 2019).

The comparison made in Figure 1B reveals that as cycling rates increase, the thermal gradient strategy yields a greater benefit for the ΔT_{cold} cells as shown by the widened gap in capacity retention during early cycling (<30 cycles) as well as the delayed crossover point at which the 20°C cells exhibit higher capacity retention than their ΔT_{cold} counterparts. Specifically, by increasing cycling rates, the number of cycles that ΔT_{cold} cells maintain higher capacity retention *versus* the 20 C cells increases from ~30 cycles at 1C|2D to ~55 cycles at 2C|3D to ~70 cycles at 4C|6D. Further, while the capacity retention of the 20°C cell suffers from each successive increase in cycling rate, the ΔT_{cold} cells demonstrate the best capacity retention in the study at intermediate cycling rates (2C|3D; 20 cycles to 80% capacity retention, 39 cycles to 50% capacity retention). One possible explanation for the intermediate cycling rates being the most favorable for capacity retention is that at the higher current densities of 4C|6D cycling, there may be limitations from cathode (de)lithiation kinetics or transport through the electrolyte at a lower thermal average.

The early cycling benefit from using the ΔT_{cold} condition can be explained in part by investigating the voltage profiles during the first charge at each C-rate. As illustrated in Figures 1C, D, ΔT_{cold} cells exhibit a larger nucleation overpotential at each rate when compared to the 20°C cells. As a point of reference, the equilibrium potential for LFP falls between 3.40 and 3.45 V for states of charge ranging from 10% to 90% as measured using current density of 51.7 μA/cm^2 and 48 h rests (Srinivasan and Newman, 2004). As a result of higher nucleation overpotential, the cells subjected to the thermal gradient are expected to deposit smaller Li nucleates with a higher density of nucleates, thereby resulting in a better seed layer of lithium on the current collector (Pei et al., 2017). As plating progresses, the increased overpotentials seen for the ΔT_{cold} cells persist as Li forms an alloy with the Au before eventually plating as metallic lithium (capacity >0.03 mA h/cm^2) (Yan et al., 2016). It is interesting to note that at 20 C, as C-rate increases, the amount of capacity required before reaching this bulk Li growth stage increases; the capacity at which the final plateau is reached shifts right from 1C to 4C. For ΔT_{cold}, at least at these C-rates, the volume of Li deposited (capacity) is insensitive to the C-rate used; the Li growth plateau always onsets by 0.37 mA h/cm^2, further suggesting that the thermal gradient approach is effective at uniformly seeding the current collector. Moreover, the ΔT_{cold} condition is favorable because its lower temperature is expected to minimize parasitic Li reactions and loss of lithium inventory (Thenuwara et al., 2019). That said, higher temperatures will cause better coalescence of Li as the plating capacity increases. As early as cycle 2, the pathway of nucleation and alloying is no longer present for cells tested with either thermal condition, as is evidenced by Figure 1C and Supplementary Figure S3D. Rather, Li plating at the anode follows an immediate plateau which persists during continued cycling as shown in Figures S3e-f. In the case of the ΔT_{cold} cells, discharge capacities increase during early cycling, likely due to the formation of this negative electrode and accumulation of self-heating in the cells.

2.2 Limitations to the thermal gradient strategy resulting from concentrated electrolytes and varied current collectors

As previously discussed, we selected the electrolyte used in this work for its low temperature behavior (Thenuwara et al., 2020), and it has been demonstrated that increased salt concentrations in electrolytes improves cycle life in LMBs (Nilsson et al., 2019). In our experiments, this trend is corroborated for both thermal conditions when using twice the concentration of LiTFSI, as is illustrated by the discharge capacity in Figure 2A and normalized discharge capacity in Figure 2B wherein cells were cycled using a 2C|3D protocol. Moreover, cycling at 20°C is favored with the increased concentration electrolyte during early cycles, a reversal from the previous trend in which ΔT_{cold} cells consistently demonstrated higher discharge capacities than their 20°C counterparts. Specifically, at higher electrolyte concentration, cells cycled at 20 C reach at ~28 cycles before fading to 50% of its initial discharge capacity whereas at lower concentration, this point was crossed at ~20 cycles. ΔT_{cold} cells exhibit a slower rate of capacity fade, likely as a function of not moving as much lithium during charge and discharge, thereby protecting continued reactions between the deposited lithium metal and electrolyte. This is further corroborated through electrochemical impedance spectroscopy (EIS), provided in Figures 2C, D for ΔT_{cold} and 20°C cells with concentrated electrolyte, respectively, which reveals that the ΔT_{cold} cells are initially more resistive and may suffer from high viscosity at low temperatures as equivalent series resistance (R_S) is higher for the concentrated ΔT_{cold} cells as compared to ones using the baseline electrolyte.

For both thermal conditions, R_S and, to a greater degree, charge transfer resistance (R_{CT}) grows in the first 10 cycles, coinciding with the rapid initial capacity fade. Supplementary Figures S4 illustrates these trends more clearly by providing R_S and R_{CT} as a function of cycle number. After those 10 cycles, the resistances grow at different rates depending on the thermal condition. R_S continues to increase steadily throughout cycling for the 20°C cell; it is hypothesized that progression of porous electrodes results in higher contact resistance and electrolyte consumption due to more SEI (and faster growth) at higher temperatures.(Maraschky and Akolkar, 2020; Thenuwara et al., 2019; Zhang et al., 2023) Our group has visually observed this phenomena and point the reader to optical cell videos of denser and more compact Li deposition on an Au/Cu current collector

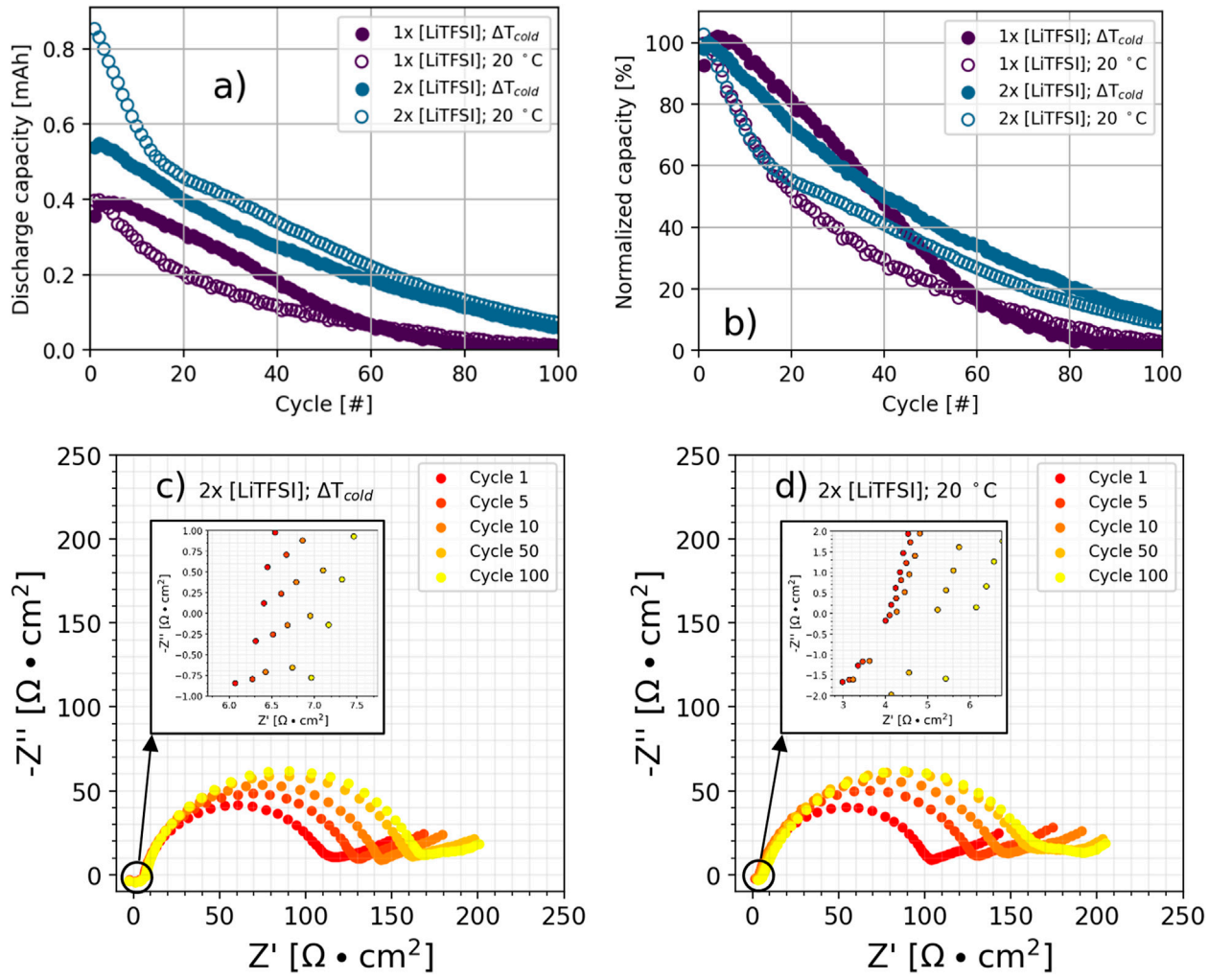

FIGURE 2
Effect of electrolyte concentration and thermal conditions on **(A)** discharge capacity and **(B)** normalized capacity during 2C|3D cycling, where baseline electrolyte composition is 0.8 M LiTFSI +0.2 M $LiNO_3$ in 80:20 DOL:DME with an additional 10 wt% FEC. In **(A)**, the height of the y-axis corresponds to 0.909 mA h, the theoretical capacity of the cathode. Potentiostatic EIS measurements for **(C)** ΔT_{cold} and **(D)** 20°C cells with 2× concentration of LiTFSI are acquired at the top of charge. All cycles conducted using 2C charge and 3C discharge.

cycled using ΔT_{cold} conditions as compared to isothermally at 20°C (Atkinson et al., 2020). In this work, this trend is particularly evident from 50 to 100 cycles, wherein the 20°C cell has a distinct low frequency arc that is normally attributed to porous Li accumulation on the anode (Liao et al., 2005; Drvarič Talian et al., 2019; Atkinson et al., 2020). This low frequency feature for ΔT_{cold} is also present, but noticeably smaller.

Electrolyte viscosity is likely limiting cycling performance for the thermal gradient condition, as ion conductivity should increase with the higher concentration of LiTFSI (Lithium bis(trifluoromethane)sulfonimide). When comparing the two thermal conditions, despite operating at a lower average temperature, the R_{CT} is similar for the ΔT_{cold} cells compared to those cycled at 20°C. After 10 cycles, the ΔT_{cold} cell exhibits a lower R_{CT}, supporting the notion that the thermal gradient reduces electrode degradation while the slower rate of R_S growth indicates a diminished rate of electrolyte consumption.

Strategies that may be beneficial independently may not be so when combined, and the overall system must be optimized for achieving improved performance. As another example, the majority of this study relies on the use of 25 nm of Au sputter coated on a Cu substrate as the anode current collector as previous reports have highlighted the favorability of plating lithium on Au rather than Cu (Yan et al., 2016). To compare the influence of overpotential based on varying the negative electrode as well as demonstrate the efficacy of the thermal gradient strategy on more practical current collectors, cells were constructed with bare Cu as the anode. Cycle life data for these tests are provided in Supplementary Figures S5; to summarize, cells without the Au coating demonstrate stable performance through 10 cycles (~95% retention) when cycling under the thermal gradient condition, while those cycled isothermally at 20°C fade to ~80% at the same point. After 10 cycles, capacity fades rapidly for the ΔT_{cold} cells as

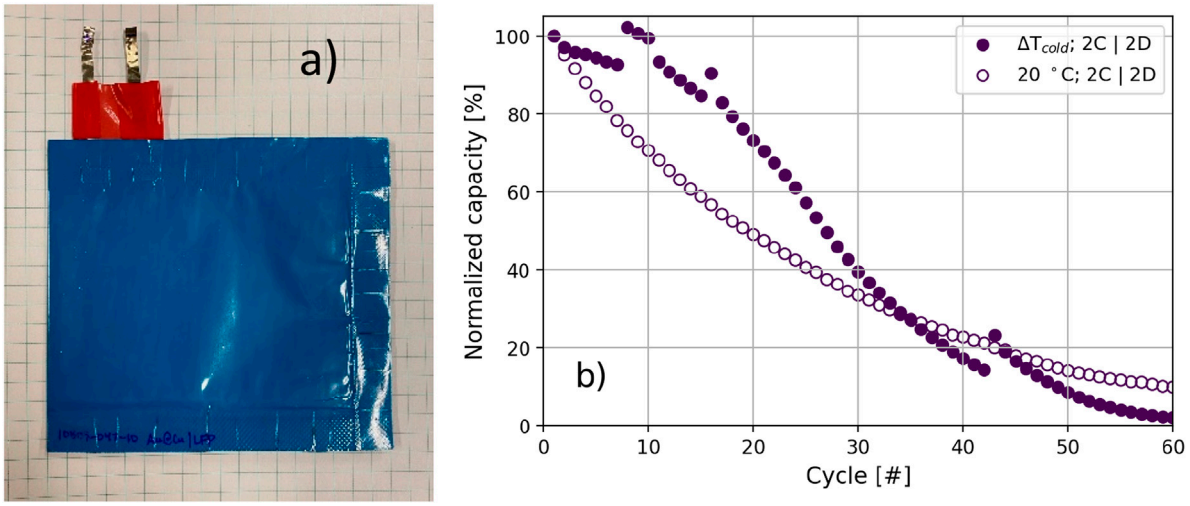

FIGURE 3
(A) Image of a representative 20 mA h pouch cell and **(B)** the corresponding performance demonstrated through normalized capacity.

compared to the steady decline exhibited by the 20°C cells, further motivating the use of thermal gradients as an effective formation strategy.

2.3 Mirrored performance in pouch cells

The form factor for battery systems plays a crucial role in determining cycling performance. To assess the viability of the thermal gradient strategy as a mechanism to improve early cycling in a more practical form factor, experiments were replicated in single-layer pouch cells. This resulted in performance trends that are comparable to those exhibited by coin cells, as shown in Figure 3B. Note that while both cell formats were characterized using both ΔT_{cold} and 20°C, the pouch cells were cycled with symmetric 2C|2D rates unlike the coin cell experiments. Despite this, the ΔT_{cold} pouch cells still demonstrate a slower rate of capacity fade during initial cycles.

Cell performance would likely continue to improve with ΔT_{cold} at an increased ratio between discharge and charge rate (Qian et al., 2016; Louli et al., 2021). Optimization of xC|yD rate is required to find the cycling conditions, which benefit most from the ΔT_{cold} strategy in the pouch cell form factor. In fact, performance differences between the two form factors, point out a limitation of the strategy not apparent in the coin cells. The lower thermal average of the cells cycled using ΔT_{cold} slows down kinetics and transport, truncated charging. Therefore, despite the better capacity retention of ΔT_{cold} Figure 3B, the delivered capacity is lower than the 20 C sample (Figure 4A). The effect is more prominent in the pouch cells, because of different thermal conductivity of the packaging and the use of a pure Cu anode. The coin cell experiments used a Au@Cu anode, resulting in different wetting and nucleation behaviors (Supplementary Figures S5). This disadvantage motivated exploring the use of the ΔT_{cold} strategy only in early cycles, leveraging minimized parasitic Li reactions during SEI formation and optimal plating nucleation. These benefits will perpetuate in subsequent cycles after the cells return to ambient conditions.

2.4 Thermal gradient as a formation strategy

The light blue triangles in Figure 4A shows the cycling behavior at 20 C after the completion of 2 cycles at ΔT_{cold}. This condition (ΔT_{cold} formation) delivers higher capacity than simply 20°C cycling, especially in the first 10 cycles. Further, the ΔT_{cold} formation cell maintains ~100% coulombic efficiency (CE) for 30 cycles, compared to ~95% CE for the 20 C one (Figure 4B). To explore the implications of the ΔT_{cold} environment on plating morphologies pouches subjected to ΔT_{cold} and ΔT_{cold} formation were opened after 5 and 100 cycles (Figures 4C, D). The high magnification photographs indicate uniform and silvery, film-like, metallic lithium plating after 5 cycles in ΔT_{cold}. Similar morphology is observed for ΔT_{cold} formation but with slightly larger feature sizes on the order of ~10 μm, indicating larger nucleates have begun to form due to the ambient temperature rise. After 100 cycles in ΔT_{cold}, the metal surface has turned grey in color, indicating accumulation of dead lithium, causing capacity loss (Figure 4A). The ΔT_{cold} formation sample also accumulates dead lithium after 100 cycles but still exhibits silvery metal nucleates. The nucleates after 100 cycles have increased in size to ~20 μm compared to the ~10 μm observed after 5 cycles. These morphological distinctions and degradation modes indicate the advantage of ΔT_{cold} cycling and the opportunity to optimize the technique for formation of ZELMB, to enable enhanced performance in practical systems.

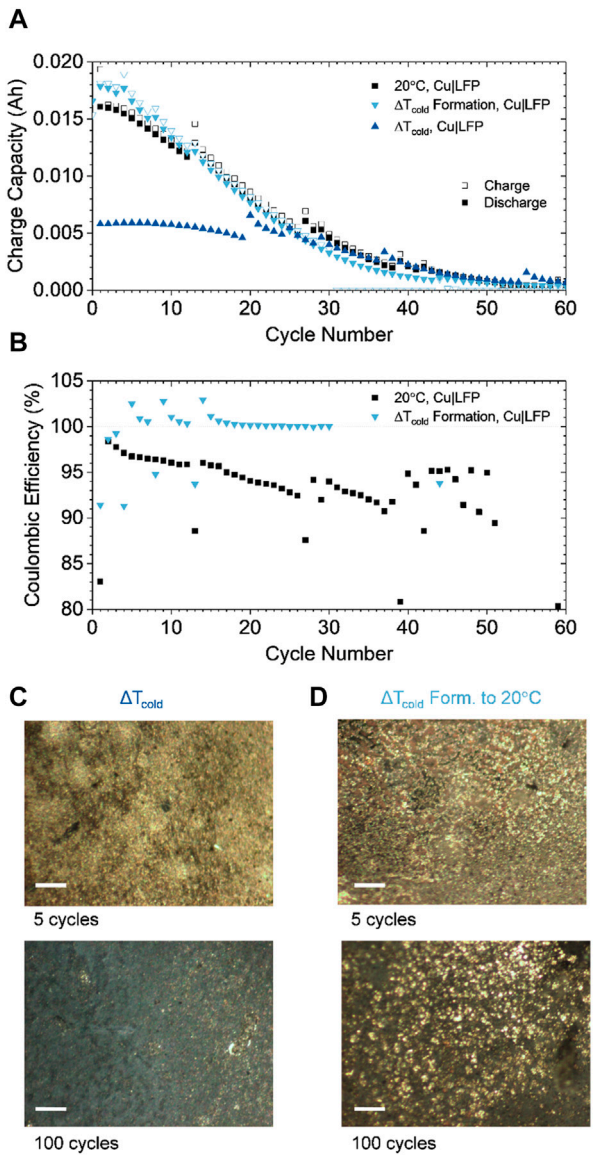

FIGURE 4
(A) Pouch cell comparison of discharge capacity during 2C|2D cycling using the thermal gradient strategy (ΔT_{cold}) and cycling at 20°C and 2 thermal gradient (ΔT_{cold}) formation cycles followed by cycling at 20°C; the height of the y-axis corresponds to 0.02 A h, the theoretical capacity of the cathode. Here, the improved relative capacity retention demonstrated in Figure 3 is achieved by formation without preventing the low temperature penalty on total discharge capacity (only ~0.005 A h for ΔT_{cold} cycling) **(B)** Coulombic efficiency of the ΔT_{cold} Formation and 20°C cells. **(C,D)** optical cell investigation of plating morphologies after 5 and 100 cycles using ΔT_{cold} and ΔT_{cold} Formation, respectively. Scale bar = 100 µm.

3 Conclusion

We demonstrate the use of a ΔT_{cold} environment, possessing a low thermal average (~6.4°C) and small thermal gradient (0.7°C), to suppress undesired Li side reactions, like SEI growth, and facilitate film like growth, which is less likely to form dendrites and more repeatable. This condition is most effective with mismatched charge and discharge rates and at charge rates faster than 1 h. The best capacity retention is observed at 3C charge and 4C discharge, a 50 min full cycle. These high charge rates are attractive for electric vehicle and portable electronic applications where fast charging is desired. Building on the improved SEI formation and plating nucleation or seeding, we demonstrate that 2 formation cycles under ΔT_{cold} conditions, followed by 20°C cycling, outperform cells simply cycled at 20°C. To realize the full potential of ΔT_{cold} formation, the number of cycles and charge and discharge rates require optimization. With the trend to use the pouch cell form factor for ZELMBs, the application of ΔT_{cold} conditions during formation is a practical approach and will provide lasting performance benefits.

4 Experimental procedures

4.1 Resource availability

Further information and requests for resources should be directed to and will be fulfilled by the lead contact, CL (corey.love@nrl.navy.mil). This study did not generate any new unique reagents. The data generated during this study is available from the lead contact upon reasonable request. This includes raw data from electrochemical tests as well as the post-processing Python or Origin scripts developed by AR and RA.

4.2 Coin cell fabrication

Experiments were performed using 93 µm thick $LiFePO_4$ (LFP, areal loading = 6.5 mg/cm^2) on a 15 µm thick Al foil as the positive electrode and 25 nm of Au sputter coated (BAL-TEC SCD 005) on a 9 µm thick Cu foil as the negative electrode. The positive and negative electrodes were cut into 0.967 and 1.58 cm^2 disks, respectively, and a single-ply separator (Entek Gold LP UHMWPE; thickness is 19.4 µm and the porosity is 37%) was cut to 17 mm in diameter; all materials were vacuum dried for >12 h at 60°C (Love, 2011). With the theoretical capacity of the LFP taken as 0.94 mA h/cm^2 based on the electrode parameters, the nominal 1C capacity for these cells is 0.909 mA h. Unless otherwise stated, the electrolyte used for each cell was 65 µL of 0.8 M LiTFSI +0.2 M $LiNO_3$ in 80:20 DOL:DME with an additional 10 wt% FEC as previously reported by Thenuwara et al. (2020) Coin cells were assembled using 2032-type parts from MTI Corp., wherein 1.2 mm total thickness of stainless steel spacers were adjacent the cathode-separator-foil stack, and a wave spring was placed in between a spacer and the negative cell can. Each condition has two representative cells as replicates; for visual clarity, the thermal conditions are displayed in figures by one of these representative cells. Pouch cell data (also featuring representative data from two replicate cells) also serves to validate reproducibility of the coin cell results in that the same trends are maintained with respect to a given thermal condition.

4.3 Pouch cell fabrication

Electrodes, electrolyte and separator materials used in the pouch cell studies were the same as those used for fabricating coin cells. The

LFP cathodes were cut to dimensions of 56 mm × 43 mm, resulting in a nominal cell capacity of 20 mA h. The 25 nm Au on Cu foil was cut to dimensions of 58 mm × 45 mm. The electrolyte volume used for each cell was 500 µL. Sealed cells, as depicted in Figure 3A, were fixtured with a c-clamp to stack pressure of ~550 kPa (~80 psi) during cycling.

4.4 Test configurations

Coin and pouch cells cycled at 20°C were tested in a Tenney isothermal chamber (TPS T2C-A-F4T) set to 20°C. Coin cells subjected to a thermal gradient were positioned between two heat exchanger plates inside the Tenney isothermal chamber. The plates were clamped to a constant pressure with a c-clamp. Pressure activated paper (Fujifilm) indicates uniform distribution of 550 kPa. Fluid was circulated through the top heat exchanger plate using a fluid circulating bath (Supplementary Figures S1A); fluid was not circulated through the bottom heat exchanger plate. The set point of the Tenney isothermal chamber was 25 C while the fluid circulating bath was set to 3 C. This configuration and set points resulted in a temperature of 6 C at the positive electrode and 6.7°C at the negative electrode (Atkinson et al., 2020; Carter et al., 2021). Thus, the average temperature of the two electrodes (i.e., thermal average) was T_{avg} = 6.35°C and the temperature difference was ΔT = 0.7°C. Dummy coin cells instrumented with thin-film thermistors (954-103JT-100, Mouser) enabled the temperature of each electrode to be precisely measured. For pouch cells subjected to thermal gradient conditions, the temperature of the two electrodes were identical to those in the coin cells, namely 6°C and 6.7°C at the positive and negative electrode, respectively. These electrode temperatures were achieved by circulating fluid through both heat exchanger plates (Supplementary Figures S1B). The set points of the circulating baths connected to the top (adjacent to the positive electrode) and bottom plates were 2.1°C and 7.9°C, respectively. Similarly, these temperatures were precisely measuring using dummy pouch cells embedded with thermistors.

4.5 Electrochemical procedures

Cells were cycled between 2.9 and 4.0 V using an 8-channel PARSTAT battery tester (AMETEK Scientific Instruments) using charge rates ranging from 1C to 4C and discharge rates ranging from 1D to 6D. Charge and discharge C-rates are noted as C/x and D/x, where x is the number of hours to complete a full charge or discharge. No formation cycles were used at the beginning of life. Electrochemical impedance spectroscopy was performed every 5 cycles for all cells in potentiostatic mode using a 10 mV RMS amplitude, frequencies logarithmically spanning 300 kHz to 0.1 Hz, and 10 points per decade. The equivalent series resistance (R_S) reported in this study refers to the intersection of the impedance spectra with the real-axis at high frequencies (>95 kHz). The charge transfer resistance (R_{CT}) refers to the local minima of the impedance spectra at low frequency (<5 Hz) minus the R_S (Atkinson et al., 2020).

4.6 Post mortem optical microscopy

Images were collected using Infinity Analyze software and a Navitar Zoom 6,000 lens apparatus with a Luminera Infinity 2 digital camera. Electrodes were imaged at ×3.38 magnification with a resolution limit of 7.67 µm.

Data availability statement

The raw data supporting the conclusions of this article will be made available by the authors, without undue reservation.

Author contributions

AR: Investigation, Software, Writing–original draft. RA: Conceptualization, Methodology, Data curation, Formal Analysis, Validation. TK: Data curation, Formal Analysis, Writing–review and editing, Investigation. RC: Data curation, Formal Analysis, Investigation, Writing–review and editing, Conceptualization, Methodology. CL: Conceptualization, Methodology, Writing–review and editing, Supervision.

Funding

The author(s) declare that no financial support was received for the research, authorship, and/or publication of this article.

Acknowledgments

The authors thank Dr. Michele Anderson at the Office of Naval Research for financial support of this work N0001422WX00855. AR acknowledges support from the American Society for Engineering Education Postdoctoral Fellowship program. TK acknowledges support from the Research Associateships Program administered by the National Research Council.

Conflict of interest

Author RA was employed by Excet, Inc.

The remaining authors declare that the research was conducted in the absence of any commercial or financial relationships that could be construed as a potential conflict of interest.

The author(s) declared that they were an editorial board member of Frontiers, at the time of submission. This had no impact on the peer review process and the final decision.

Publisher's note

All claims expressed in this article are solely those of the authors and do not necessarily represent those of their affiliated organizations, or those of the publisher, the editors and the reviewers. Any product that may be evaluated in this article, or claim that may be made by its manufacturer, is not guaranteed or endorsed by the publisher.

Supplementary material

The Supplementary Material for this article can be found online at: https://www.frontiersin.org/articles/10.3389/fenrg.2024.1327955/full#supplementary-material

References

Atkinson, R. W., Carter, R., and Love, C. T. (2019). Operational strategy to stabilize lithium metal anodes by applied thermal gradient. *Energy Storage Mater.* 22, 18–28. doi:10.1016/j.ensm.2019.07.021

Atkinson, R. W., Kingston, T. A., Klein, E. J., Newringeisen, A., Carter, R., and Love, C. T. (2020). Minimizing lithium deactivation during high-rate electroplating via sub-ambient thermal gradient control. *Mater. Today Energy* 18, 100538. doi:10.1016/j.mtener.2020.100538

Carter, R., Kingston, T. A., Atkinson, R. W., Parmananda, M., Dubarry, M., Fear, C., et al. (2021). Directionality of thermal gradients in lithium-ion batteries dictates diverging degradation modes. *Cell Rep. Phys. Sci.* 2 (3), 100351. doi:10.1016/j.xcrp.2021.100351

Carter, R., and Love, C. T. (2018). Modulation of lithium plating in Li-ion batteries with external thermal gradient. *ACS Appl. Mater. Interfaces* 10 (31), 26328–26334. doi:10.1021/acsami.8b09131

Chang, W., Bommier, C., Mohr, R., and Steingart, D. (2021). Impact of non-arrhenius temperature behavior on the fast-charging capabilities of LiCoO2–graphite lithium-ion batteries. *J. Phys. Chem. C* 125 (3), 1731–1741. doi:10.1021/acs.jpcc.0c09972

Drvarič Talian, S., Bobnar, J., Sinigoj, A. R., Humar, I., and Gaberšček, M. (2019). Transmission line model for description of the impedance response of Li electrodes with dendritic growth. *J. Phys. Chem. C* 123 (46), 27997–28007. doi:10.1021/acs.jpcc.9b05887

Genovese, M., Louli, A. J., Weber, R., Martin, C., Taskovic, T., and Dahn, J. R. (2019). Hot Formation for improved low temperature cycling of anode-free lithium metal batteries. *J. Electrochem. Soc.* 166 (14), A3342–A3347. doi:10.1149/2.0661914jes

Hatzell, K. B. (2023). Anode-less or anode-free? *ACS Energy Lett.* 8 (11), 4775–4776. doi:10.1021/acsenergylett.3c02163

Liao, X.-Z., Ma, Z.-F., He, Y.-S., Zhang, X.-M., Wang, L., and Jiang, Y. (2005). Electrochemical behavior of LiFePO[sub 4]/C cathode material for rechargeable lithium batteries. *J. Electrochem. Soc.* 152 (10), A1969. doi:10.1149/1.2008988

Lohrberg, O., Voigt, K., Maletti, S., Auer, H., Nikolowski, K., Heubner, C., et al. (2023). Benchmarking and critical design considerations of zero-excess Li-metal batteries. *Adv. Funct. Mater.* 33 (24), 2214891. doi:10.1002/adfm.202214891

Louli, A. J., Coon, M., Genovese, M., deGooyer, J., Eldesoky, A., and Dahn, J. R. (2021). Optimizing cycling conditions for anode-free lithium metal cells. *J. Electrochem. Soc.* 168 (2), 020515. doi:10.1149/1945-7111/abe089

Love, C. T. (2011). Thermomechanical analysis and durability of commercial micro-porous polymer Li-ion battery separators. *J. Power Sources* 196 (5), 2905–2912. doi:10.1016/j.jpowsour.2010.10.083

Love, C. T., Baturina, O. A., and Swider-Lyons, K. E. (2014). Observation of lithium dendrites at ambient temperature and below. *ECS Electrochem. Lett.* 4 (2), A24–A27. doi:10.1149/2.0041502eel

Maraschky, A., and Akolkar, R. (2020). Temperature dependence of dendritic lithium electrodeposition: a mechanistic study of the role of transport limitations within the SEI. *J. Electrochem. Soc.* 167 (6), 062503. doi:10.1149/1945-7111/ab7ce2

Mistry, A., Fear, C., Carter, R., Love, C. T., and Mukherjee, P. P. (2019). Electrolyte confinement alters lithium electrodeposition. *ACS Energy Lett.* 4 (1), 156–162. doi:10.1021/acsenergylett.8b02003

Nanda, S., Gupta, A., and Manthiram, A. (2020). Anode-Free full cells: a pathway to high-energy density lithium-metal batteries. *Adv. Energy Mater.* 11 (2). doi:10.1002/aenm.202000804

Nilsson, V., Kotronia, A., Lacey, M., Edström, K., and Johansson, P. (2019). Highly concentrated LiTFSI–EC electrolytes for lithium metal batteries. *ACS Appl. Energy Mater.* 3 (1), 200–207. doi:10.1021/acsaem.9b01203

Park, C.-Y., Kim, J., Lim, W.-G., and Lee, J. (2023). Toward maximum energy density enabled by anode-free lithium metal batteries: recent progress and perspective. *Exploration* n/a (n/a), 20210255. doi:10.1002/EXP.20210255

Pei, A., Zheng, G., Shi, F., Li, Y., and Cui, Y. (2017). Nanoscale nucleation and growth of electrodeposited lithium metal. *Nano Lett.* 17 (2), 1132–1139. doi:10.1021/acs.nanolett.6b04755

Qian, J., Adams, B. D., Zheng, J., Xu, W., Henderson, W. A., Wang, J., et al. (2016). Anode-Free rechargeable lithium metal batteries. *Adv. Funct. Mater.* 26 (39), 7094–7102. doi:10.1002/adfm.201602353

Srinivasan, V., and Newman, J. (2004). Discharge model for the lithium iron-phosphate electrode. *J. Electrochem. Soc.* 151 (10), A1517. doi:10.1149/1.1785012

Thenuwara, A. C., Shetty, P. P., Kondekar, N., Sandoval, S. E., Cavallaro, K., May, R., et al. (2020). Efficient low-temperature cycling of lithium metal anodes by tailoring the solid-electrolyte interphase. *ACS Energy Lett.* 5, 2411–2420. doi:10.1021/acsenergylett.0c01209

Thenuwara, A. C., Shetty, P. P., and McDowell, M. T. (2019). Distinct nanoscale interphases and morphology of lithium metal electrodes operating at low temperatures. *Nano Lett.* 19 (12), 8664–8672. doi:10.1021/acs.nanolett.9b03330

Wang, J., Huang, W., Pei, A., Li, Y., Shi, F., Yu, X., et al. (2019). Improving cyclability of Li metal batteries at elevated temperatures and its origin revealed by cryo-electron microscopy. *Nat. Energy* 4, 664–670. doi:10.1038/s41560-019-0413-3

Yan, K., Lu, Z., Lee, H.-W., Xiong, F., Hsu, P.-C., Li, Y., et al. (2016). Selective deposition and stable encapsulation of lithium through heterogeneous seeded growth. *Nat. Energy* 1 (3), 16010. doi:10.1038/nenergy.2016.10

Yan, K., Wang, J., Zhao, S., Zhou, D., Sun, B., Cui, Y., et al. (2019). Temperature-dependent nucleation and growth of dendrite-free lithium metal anodes. *Angew. Chem.* 131 (33), 11486–11490. doi:10.1002/ange.201905251

Yang, Y., Davies, D. M., Yin, Y., Borodin, O., Lee, J. Z., Fang, C., et al. (2019). High-efficiency lithium-metal anode enabled by liquefied gas electrolytes. *Joule* 3 (8), 1986–2000. doi:10.1016/j.joule.2019.06.008

Zhang, S., Cheng, B., Fang, Y., Dang, D., Shen, X., Li, Z., et al. (2022). Inhibition of lithium dendrites and dead lithium by an ionic liquid additive toward safe and stable lithium metal anodes. *Chin. Chem. Lett.* 33 (8), 3951–3954. doi:10.1016/j.cclet.2021.11.024

Zhang, S., Ding, J.-F., Xu, R., Xiao, Y., Yan, C., and Huang, J.-Q. (2023). Temperature-mediated dynamic lithium loss and its implications for high-efficiency lithium metal anodes. *Adv. Energy Mater.* 2303726. doi:10.1002/aenm.202303726

Zhao, P., Pan, J., Zhang, D., Tang, Y., Tai, Z., Liu, Y., et al. (2023). Designs of anode-free lithium-ion batteries. *Batteries* 9 (7), 381. doi:10.3390/batteries9070381